Journal of Biological Engineering

RESEARCH

Open Access

Core-shell nanofiber dressings with zinc oxide nanoparticles and cell-free fat extract: boosting fibroblast activity and antibacterial efficacy

Aydin Mahmoudnezhad[1], Mahsa Bayrami[2], Mahdiyeh Saadati[3], Yavuz Nuri Ertaş[4], Mozhgan Abasi[5], Aylar Ebrahimi[6] and Younes Pilehvar[6*]

Abstract

Background This study presents the development and characterization of innovative core-shell nanofiber wound dressings incorporating zinc oxide nanoparticles (nZnO) and cell-free fat extract (CEFFE) to enhance fibroblast activity and antibacterial efficacy.

Results CEFFE was prepared and analyzed, revealing high concentrations of essential growth factors, particularly bFGF and TGF-β1, supporting its therapeutic potential in tissue regeneration. The fabricated nanofibers (PLCL, nZnO/PLCL, PLCL-CEFFE/HA, and nZnO/PLCL-CEFFE/HA) were examined using FE-SEM and TEM, demonstrating successful encapsulation and morphological variations due to nZnO incorporation. XRD analysis confirmed the structural integrity and effective loading of nZnO and CEFFE. Hydrophilicity assessment via water contact angle measurements showed that CEFFE/HA significantly enhanced the hydrophilicity of PLCL membranes, crucial for wound exudate management. Mechanical tests indicated that CEFFE/HA addition maintained the scaffold's mechanical robustness, while nZnO slightly reduced mechanical properties. In vitro release studies revealed a biphasic release pattern of Zn^{2+} ions and growth factors from nZnO/PLCL-CEFFE/HA nanofibers, ensuring prolonged antibacterial activity and sustained therapeutic effects. Antibacterial assays demonstrated significant efficacy against *E. coli* and *S. aureus*, attributed to nZnO. MTT assays and FE-SEM analysis confirmed enhanced NIH-3T3 cell proliferation and adhesion on PLCL-CEFFE/HA nanofibers due to the controlled release of growth factors. The scratch assay showed superior cell migration and wound healing potential for PLCL-CEFFE/HA formulations.

Conclusions These findings underscore the potential of nZnO/PLCL-CEFFE/HA core-shell nanofibers as multifunctional wound dressings, combining antibacterial properties with enhanced tissue regeneration capabilities. However, further studies are needed to assess long-term stability and in vivo performance, which represent key challenges for future research.

Keywords Core-shell nanofiber, Wound dressing, Zinc oxide nanoparticles, Cell-free fat extract

*Correspondence:
Younes Pilehvar
ypilehvar@umsu.ac.ir

Full list of author information is available at the end of the article

Background

Wound healing is a critical and intricate biological process aimed at restoring skin and tissue integrity following injury. This multifaceted process is typically divided into four stages: hemostasis, inflammation, proliferation, and remodeling. In chronic wounds, such as diabetic ulcers, venous leg ulcers, and pressure ulcers, one or more of these stages can stall, resulting in prolonged healing, an increased risk of infection, and significant patient morbidity. These wounds present not only a physical burden to the patient but also an economic challenge to healthcare systems due to the prolonged care and associated risks of complications [1].

The traditional approach to wound management has long relied on the use of basic dressings, such as gauzes, hydrogels, and hydrocolloids. These dressings primarily serve to maintain a moist wound environment, absorb exudate, and offer a physical barrier against microbial threats. However, despite their ability to support some aspects of healing, these dressings lack the bioactive properties necessary to address the complex pathologies of chronic wounds. For instance, they are not typically equipped to deal with impaired cellular functions, high microbial loads, or the need for enhanced tissue regeneration [2, 3]. Similarly, hydrogels offer excellent moisture retention and biocompatibility, fostering an optimal healing environment. However, limitations in mechanical strength and scalability pose challenges for chronic wound management, particularly in large or irregular wound areas [4]. As a result, modern wound care has increasingly focused on advanced wound dressings that incorporate bioactive agents capable of addressing the specific needs of chronic wound healing, such as infection control and tissue regeneration.

In the quest for more effective treatments, researchers have explored the use of antimicrobial nanoparticles. Among these, silver nanoparticles (AgNPs) are perhaps the most widely studied due to their potent ability to disrupt bacterial membranes, inhibit cellular respiration, and induce oxidative stress in pathogens [5, 6]. AgNP-based wound dressings have shown impressive efficacy against a broad range of pathogens, including antibiotic-resistant bacteria. However, despite their antimicrobial prowess, concerns have arisen over their potential cytotoxicity and the possibility of inducing bacterial resistance when used over extended periods. This has led to a growing interest in finding safer alternatives that can offer comparable antimicrobial protection without these associated risks [7, 8].

Zinc oxide nanoparticles (nZnO) have emerged as one of the most promising alternatives to AgNPs. Like silver, zinc oxide possesses strong antimicrobial properties, acting through the generation of reactive oxygen species (ROS) and the disruption of bacterial cell membranes [9]. Unlike AgNPs, however, nZnO have demonstrated significantly lower cytotoxicity, making them more suitable for long-term use. Moreover, nZnO are less likely to contribute to bacterial resistance, further enhancing their appeal as a safer antimicrobial agent in chronic wound management [7, 10].

Despite the advantages of nZnO, these nanoparticles do not inherently promote tissue regeneration, a critical factor for complete wound healing. Tissue regeneration requires the proliferation of fibroblasts, the deposition of ECM, and angiogenesis, all of which are essential for restoring the structure and function of damaged tissue. To overcome this limitation, recent research has focused on combining nZnO with bioactive compounds that can support both antimicrobial activity and tissue regeneration.

Recent advances in nanotechnology have facilitated the development of nanofiber-based wound dressings, which offer several advantages over traditional dressings. Nanofibers, typically produced through techniques like electrospinning, closely mimic the structure of the natural extracellular matrix, providing an ideal environment for cell adhesion, proliferation, and migration [11, 12]. Nanofibers also possess high porosity, which allows for effective gas exchange and exudate absorption, making them particularly well-suited for use in wound dressings [13].

One of the key benefits of nanofibers is their ability to incorporate a wide range of bioactive agents, including nanoparticles, growth factors, and proteins, to enhance both antimicrobial and regenerative functions. For instance, electrospun nanofibers loaded with nZnO have been shown to exhibit strong antibacterial properties, while also offering mechanical stability and biocompatibility [14]. In one study, polycaprolactone (PCL) nanofibers loaded with nZnO exhibited enhanced antibacterial efficacy without compromising their biocompatibility, making them a promising option for wound care applications [15]. However, these nanofibers still lacked the bioactive components necessary to actively promote tissue regeneration. Güldiken et al. [16] showed that ZnO microparticle-loaded nanocomposite thin films can enhance thermal stability and mechanical strength, along with the promotion of fibroblast viability, suggesting their potential to outperform traditional wound dressings. Furthermore, ZnO nanofibrous composites integrated with bioactive compounds have been shown to improve wound healing rates and prevent bacterial infections, showcasing their utility in clinical applications [17].

A novel and promising addition to the field of wound healing is the use of cell-free fat extract (CEFFE), which is derived from adipose tissue. CEFFE contains a rich array of growth factors, cytokines, and bioactive molecules that are known to promote angiogenesis, ECM deposition, and fibroblast proliferation. These bioactive molecules

help modulate inflammation, stimulate resident stem cells, and encourage tissue regeneration, all of which are critical for wound healing, especially in chronic wounds that have stalled in the healing process. Moreover, the antioxidant properties of CEFFE protect cells from oxidative stress, further promoting a favorable environment for wound healing [18, 19].

Despite its potential, the use of CEFFE in wound care remains underexplored. Its instability in wound environments and its susceptibility to degradation have limited its application. However, the integration of CEFFE into nanofiber-based wound dressings, particularly in core-shell nanofiber designs, might offer a solution to these challenges. By incorporating CEFFE into the core of a core-shell nanofiber structure, the bioactive molecules can be protected from degradation and released in a controlled manner, ensuring sustained regenerative activity at the wound site.

The core-shell nanofiber design presents a unique opportunity to combine the antimicrobial properties of nZnO with the regenerative capabilities of CEFFE in a single multifunctional dressing. In this design, the shell is composed of poly(l-lactide-co-ε-caprolactone) (PLCL), a copolymer that provides mechanical stability and biocompatibility, while also offering a sustained release of nZnO for prolonged antimicrobial activity. The core, made of hyaluronic acid (HA) and loaded with CEFFE, serves as a reservoir for bioactive molecules that promote tissue regeneration. This dual-layer structure can protect the sensitive bioactive agents within CEFFE, while allowing for their controlled release at the wound site.

Core-shell nanofibers have already shown promise in a variety of biomedical applications, including drug delivery and tissue engineering [20, 21]. By incorporating both nZnO and CEFFE into a core-shell nanofiber dressing, we aim to create a multifunctional dressing that can address both infection control and tissue regeneration, thereby accelerating the healing process in chronic wounds.

Materials and methods

Materials

Poly(L-lactide-co-ε-caprolactone) (PLCL, Mw = 300,000 g/mol), Hyaluronic acid (HA, Mw = 1.5×10^6 Da), hexafluoroisopropanol (HFIP) of high purity (≥ 99%) and bicinchoninic acid (BCA) protein assay kit were obtained from Sigma-Aldrich (St. Louis, MO, USA). Zinc Oxide nanoparticles (nZnO, particle size < 50 nm) was purchased from Aladdin Reagent Co. (Shanghai, China). Enzyme-linked immunosorbent assay (ELISA) kits for basic fibroblast growth factor (bFGF), transforming growth factor-β1 (TGF-β1), and vascular endothelial growth factor (VEGF) were obtained from R&D Systems (Minneapolis, MN, USA).

Preparation and characterization of CEFFE

SEME Cell Technology Co., Ltd. (Shanghai, China) supplied CEFFE, which was isolated from fresh adipose tissues in accordance with earlier instructions (Fig. 1) [22]. To put it briefly, blood and tissue fragments were

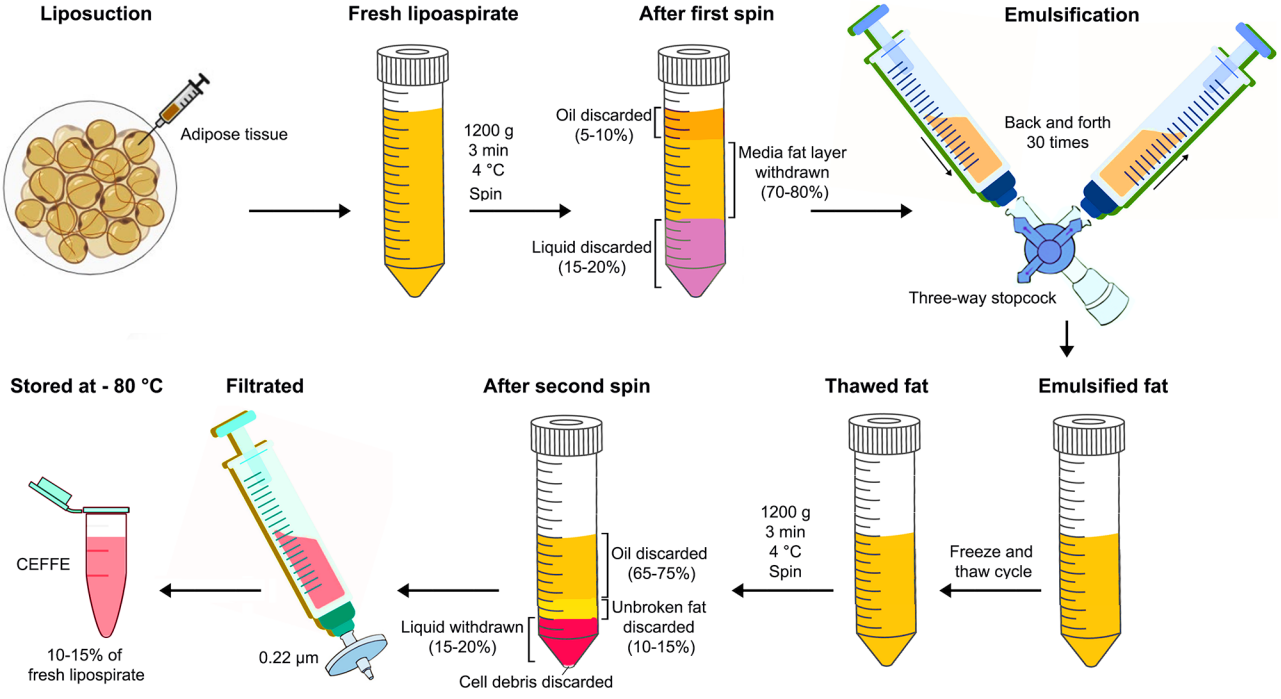

Fig. 1 Schematic illustration of the CEFFE preparation

removed from adipose tissues by rinsing them with physiological saline solution. Three layers were created after centrifugation at 1200 g for three minutes. The middle fat layer was kept for mechanical emulsification by switching between two 10-mL syringes that were connected to a three-way stopcock with an internal diameter of 2 mm thirty times. The upper oil layer and the lower aqueous layer were eliminated. After that, the emulsified fat was frozen, kept at -80 °C, and quickly thawed at 37 °C to rupture the cell membranes. Four layers formed when materials were centrifuged at 1200 g for five minutes following a single freeze-thaw cycle. In order to produce CEFFE, which was frozen at -80 °C for future research, the third liquid layer was lastly gathered and filtered using a 0.22-µm filtration membrane (Corning Glass Works, Corning, NY, USA) to eliminate bacteria and other debris. With the use of a bicinchoninic acid test kit, the protein concentration in CEFFE was calculated.

Fabrication and characterization of nZnO/PLCL-CEFFE/PVA core-shell electrospun nanofibers

For making shell solutions, PLCL 8% (w/v) was dissolved in HFIP and kept on stirring overnight under room temperature, and 2% w/w nZnO were added into PLCL solution followed by sonication for complete dispersion [23].

As the core solution, CEFFE and a 5% HA solution were well combined at a volume ratio of 7:3. The shell and core solutions had fluid flow rates of 1.0 and 0.2 mL/h, respectively. There was 15 cm separating the spinneret from the collection and a high DC voltage of 20 kV applied. Every electrospinning procedure was carried out at 27 °C and 60% relative humidity. For 72 h, the nZnO/PLCL-CEFFE/HA core-shell electrospun mats were vacuum-dried. The detailed fabricating process is illustrated in Fig. 2.

The surface morphology of the fiber membrane was examined using field emission scanning electron microscopy (FE-SEM, MIRA3 TESCAN, Czech Republic). To determine the average fiber diameters, one hundred nanofibers were randomly selected from the FE-SEM images and analyzed with Image J software (National Institutes of Health, USA). The core-shell structure and the inclusion of nZnO within individual nanofibers were identified through transmission electron microscopy (TEM, JEM-2100, JEOL, Japan). X-ray diffraction (XRD) was employed to verify the presence of nZnO. XRD measurements were conducted over a 2θ range of 10° to 80° using a Bruker D8 ADVANCE model (Germany) with CuKα radiation at 8.04 keV and a wavelength of 1.54 Å.

The surface hydrophilicity of the fiber membranes was assessed by measuring the water contact angle with a contact angle measurement instrument (DSA30, Kruss, Germany). The mechanical properties of PLCL, nZnO/PLCL, PLCL-CEFEE/HA, and nZnO/PLCL-CEFEE/HA were evaluated using the Universal Materials Testing Machine (H5K–S, Hounsfield, UK) under ambient

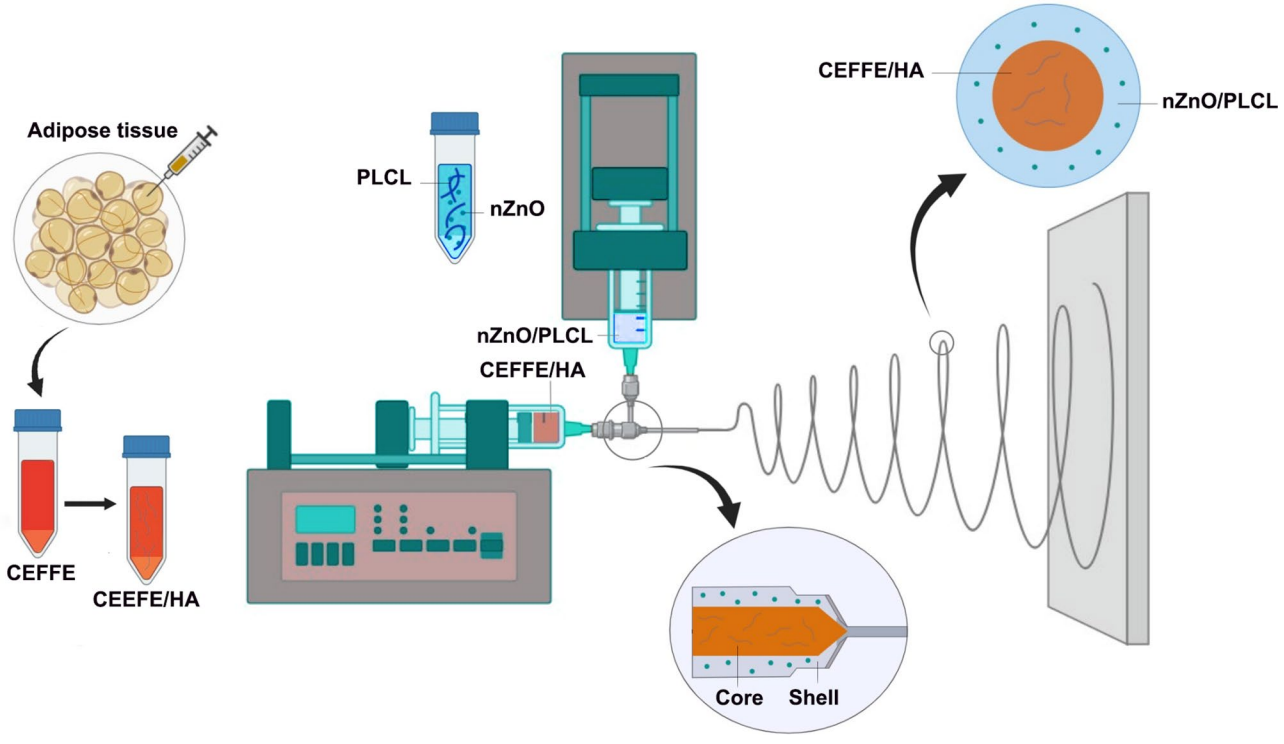

Fig. 2 Schematic illustration of fabrication process for the electrospun core-shell nanofibrous mats

conditions of 20 °C and 65% humidity. All specimens (50 mm × 10 mm, $n = 5$) were tested at a crosshead speed of 10 mm/min until failure. Prior to testing, the thickness of each specimen was measured with a digital gauge meter, accurate to 1 μm.

In vitro release of nZnO and growth factors

In this study, the release of nZnO was measured using an inductively coupled plasma atomic emission spectrometer (ICP-AES, Perkin-Elmer Optima 2000, USA). The release medium was PBS, and approximately 20 mg of the sample was placed in 4 mL of PBS. At various time intervals, 2 mL of the medium was removed and replaced with fresh PBS. The collected samples were stored at -20 °C until the Zn ion release was analyzed.

Besides, the in vitro release of growth factors present in the CEFFE from nZnO/PLCL-CEFFE/HA core-shell nanofibers was investigated. The nanofibers were cut into uniform samples of 1 cm x 1 cm and placed in 2 mL of PBS in 15 mL conical tubes, which were incubated at 37 °C with gentle shaking. At predetermined time points (0, 6, 12, 24, 48, 72, and 96 h), 1 mL of the release medium was collected and replaced with fresh PBS to maintain sink conditions. The concentrations of bFGF, TGF-β1, and VEGF in the collected samples were quantified using ELISA kits. The cumulative release of each growth factor was calculated and plotted over the 96-hour period, with data represented as mean ± standard deviation from triplicate samples.

Antibacterial activity

Antibacterial efficacy (%) was assessed using the turbidity measurement method. PLCL, nZnO/PLCL, PLCL-CEFFE/HA, and nZnO/PLCL-CEFFE/HA nanofibers were cut into 50 mg pieces and sterilized under UV light for 4 h prior to antibacterial testing. LB broth liquid culture media was prepared following the manufacturer's instructions to culture *E. coli* (BCRC 10314) and *S. aureus* (BCRC 10823) strains, sourced from the Bioresource Collection and Research Center (Hsinchu, Taiwan). A single colony of each strain was transferred to the liquid medium under sterile conditions and incubated at 37 °C with shaking (100 rpm) for 24 h. The media was then diluted to achieve a final optical density (OD) of 0.5. For each strain, sets of test tubes were prepared, each containing 5 mL of culture media and 100 μL of bacterial culture. The fiber membranes (PLCL, nZnO/PLCL, PLCL-CEFFE/HA, and nZnO/PLCL-CEFFE/HA) were placed in the test tubes, which were then incubated at 37 °C with shaking for 24 h. After the incubation period, OD was measured at 600 nm, and the antibacterial activity of each fiber membrane was calculated. The OD readings were corrected by subtracting the OD of the blank culture media. Since OD is proportional to the number of bacteria, antibacterial activity (%) was calculated using the specified equation.

Antibacterial activity (%) = (Ic – Is) / Ic × 100.

Where Ic is the OD of the control group and Is is the OD of the experimental group.

In vitro cell culture, proliferation and adhesion assays

NIH-3T3 cells (ATCC, Manassas, VA, USA) were cultured in Dulbecco's Modified Eagle's Medium (DMEM) supplemented with 10% fetal bovine serum (FBS) and 1% antibiotic-antifungal agent, maintained in a 5% CO_2 atmosphere at 37 °C, with the medium being replaced every other day. Fiber membrane samples were placed in 24-well plates and secured with stainless steel rings. Prior to cell seeding, the fiber membranes were sterilized under UV light for 12 h, washed three times with PBS, and then incubated with high glucose medium for 2 h.

To assess the cytocompatibility and proliferation of NIH-3T3 cells on the fabricated fiber membranes, an MTT assay was conducted. NIH-3T3 cells were seeded at a density of 1×10^4 cells per well in a 96-well plate containing different fiber membranes, including Control, PLCL, nZnO/PLCL, PLCL-CEFFE/HA, and nZnO/PLCL-CEFFE/HA. The cells were cultured for 1, 3, and 7 days at 37 °C in a humidified atmosphere with 5% CO_2. At each time point, 20 μL of MTT solution (5 mg/mL in PBS) was added to each well, followed by incubation for 4 hours to allow the formation of formazan crystals. Subsequently, the medium was carefully removed, and 150 μL of dimethyl sulfoxide (DMSO) was added to dissolve the formazan crystals. The OD was measured at 570 nm using a microplate reader. The experiments were performed in triplicate.

Besides, the adhesion of NIH-3T3 cells seeded on the scaffolds were visualized using FE-SEM. After 4 and 7 days of culture, the NIH-3T3 cells were fixed with 4% paraformaldehyde for 30 min at room temperature. The fixed cells were then washed with PBS and subsequently dehydrated through a graded ethanol series (30%, 50%, 70%, 90%, and 100%) for 10 min at each concentration. After dehydration, the samples were critical-point dried and sputter-coated with a thin layer of gold to enhance conductivity. FE-SEM images were captured to observe the morphology and adhesion of the cultured cells on the scaffolds.

In vitro scratch test

An *in vitro* scratch assay was conducted to assess the impact of the fibers on in vitro cell migration. After being seeded into 24-well plates, NIH-3T3 cells were cultivated to form a confluent monolayer. Next, using a p200 pipette tip to scrape the cell monolayer, a scratch was made in each well. After giving the cells a gentle culture medium wash, each well was cultured with 1 mL of low-serum

medium. With the exception of having a low FBS concentration of 1% (v/v), the low-serum medium is identical to the full medium. Then, each well received a transwell that had 100 mL of hydrogel put into it. Using a microscope (Leica DMI3000), images of each sample were taken at 0 h and after 48 h of culture. Image J software (NIH) was then used to do quantitative analysis. The following formula was used to determine each well's proportion of wound surface:

$$\begin{aligned} &Wound\ area\ (\%) \\ &= Wound\ area\ after\ 24\ h/ \\ &Wound\ area\ in\ the\ initial\ moment\ \times\ 100 \end{aligned}$$

Statistical analysis

All values were expressed as mean ± standard deviation (SD) of at least three experiments and compared using two-way ANOVA tests through GraphPad Prism 9.0 (GraphPad Software, Inc., San Diego, CA). Values of $p < 0.05$ were considered as significant.

Results and discussion

Preparation and characterization of CEFFE

The total protein concentration of CEFFE was measured by BCA, and the concentration of various factors (bFGF, TGF-β1, HGF, VGEF, BDNF, PDGF, EGF and NT-3) was measured by ELISA (Fig. 3). The total CEFFE protein concentration was found to be 4.855 ± 0.751 μg/mL. Besides, the results of ELISA indicated that bFGF was the most abundant growth factor in CEFFE, with a concentration of approximately 33.5 ng/mL. TGF-β1 was also present in significant amounts, showing a concentration of roughly 29.4 ng/mL. The concentration of HGF was observed to be around 15.2 ng/mL, while VEGF was present at approximately 12 ng/mL. Other growth factors including, BDNF, PDGF, EGF and NT-3 were found in lower concentrations.

The successful extraction and characterization of CEFFE from fresh adipose tissues represent a crucial step towards harnessing its therapeutic potential for tissue regeneration. Our study demonstrates that CEFFE is rich in various growth factors essential for tissue repair and regeneration.The substantial concentration of bFGF within CEFFE highlights its significance in promoting cellular proliferation, angiogenesis, and tissue remodeling [24]. Additionally, the presence of TGF-β1, a key regulator of extracellular matrix synthesis and chondrogenesis, underscores the potential of CEFFE in promoting articular cartilage regeneration [25]. HGF, known for its mitogenic and anti-apoptotic properties, further enhances the regenerative capacity of CEFFE by promoting cell survival and tissue repair.

Moreover, the presence of angiogenic factors such as VEGF within CEFFE suggests its potential to stimulate neovascularization, facilitating the delivery of nutrients and oxygen to the regenerating tissue [26]. This angiogenic activity is crucial for the establishment of a conducive microenvironment for tissue regeneration, particularly in avascular regions such as articular cartilage.

Although PDGF and EGF were found in relatively lower concentrations compared to other growth factors, their presence is noteworthy due to their roles in promoting cell migration, proliferation, and wound healing [24]. Despite their lower abundance, PDGF and EGF contribute to the overall regenerative potential of CEFFE, complementing the actions of other growth factors. On the other hands, BDNF and NT-3 are neurotrophic factors that support the survival and differentiation of neurons. Their presence, although in lower concentrations, indicates that CEFFE might also have a role in nerve regeneration, which can be beneficial in wounds involving nerve damage.

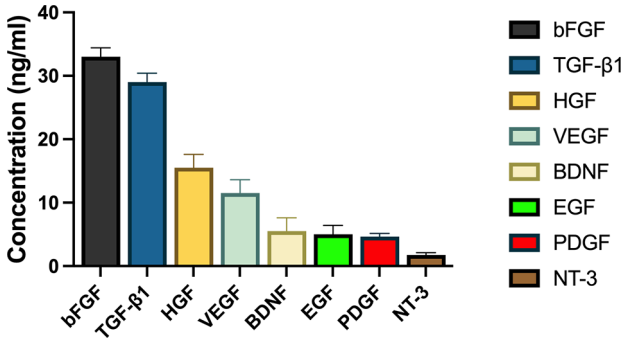

Fig. 3 The concentration of various growth factors in CEFFE detected by ELISA ($n = 3$)

Fabrication and physicochemical characterization

The concentration of 2% w/w nZnO in PLCL was selected based on previous studies that demonstrated effective antibacterial activity and biocompatibility at this level. Research has shown that ZnO nanoparticles at concentrations between 1 and 3% in polymer matrices provide enhanced surface roughness and bioactivity without compromising the structural integrity of the fibers [27, 28]. Furthermore, higher concentrations of ZnO nanoparticles tend to lead to excessive particle aggregation, which could negatively impact fiber morphology, as well as reduce the mechanical properties of the electrospun mats. By keeping the concentration at 2%, we aimed to balance the antimicrobial benefits of nZnO while minimizing aggregation and maintaining the fiber's mechanical and structural properties. Besides, the 7:3 ratio of CEFFE to HA in the core solution was chosen based on preliminary studies and existing literature [29], which suggest that this ratio maximizes the biological

activity of CEFFE while ensuring sufficient viscosity and electrospinnability of the solution. CEFFE contains bioactive components such as lipids, proteins, and growth factors, which are crucial for promoting tissue regeneration and wound healing. However, an excessive amount of CEFFE can decrease solution stability and impede the electrospinning process. The addition of 5% HA solution serves as a stabilizing agent that aids in maintaining solution viscosity, facilitating smoother fiber formation during electrospinning. This ratio has been optimized to ensure both successful coaxial electrospinning and the biological efficacy of CEFFE.

FE-SEM was utilized to analyze the surface morphology of the fabricated nanofibrous membranes (Fig. 4A), revealing significant differences among the four types: PLCL, nZnO/PLCL, PLCL-CEFFE/HA, and nZnO/PLCL-CEFFE/HA. The FE-SEM images illustrate a web-like structure across all samples, characteristic of electrospun nanofibers. However, the incorporation of nZnO has a marked impact on surface morphology and fiber diameter.

The PLCL and PLCL-CEFFE/HA membranes exhibit smooth surfaces, indicating uniform fiber formation during electrospinning. In contrast, the nZnO/PLCL and nZnO/PLCL-CEFFE/HA membranes display visible particle aggregation on the fiber surface, resulting in a rougher texture. This roughness can be attributed to the presence of nZnO, which tend to aggregate, as corroborated by previous studies [30, 31], where nanoparticle incorporation led to similar surface modifications.

The frequency histograms of fiber diameter distributions further underscore the impact of nZnO (Fig. 4B). PLCL and PLCL-CEFFE/HA membranes show relatively narrow diameter distributions centered around 400–500 nm. In contrast, the presence of nZnO in nZnO/PLCL and nZnO/PLCL-CEFFE/HA results in broader distributions with higher average diameters, extending up to 700 nm and 800 nm, respectively. These observations align with the findings of previous works [32, 33], where nanoparticle addition generally increased fiber diameters due to alterations in solution viscosity and electrospinning dynamics.

TEM provided insights into the internal fiber morphology and nanoparticle distribution (Fig. 4C). TEM images confirm the successful encapsulation of nZnO within the fiber matrix and on the surface, appearing both as

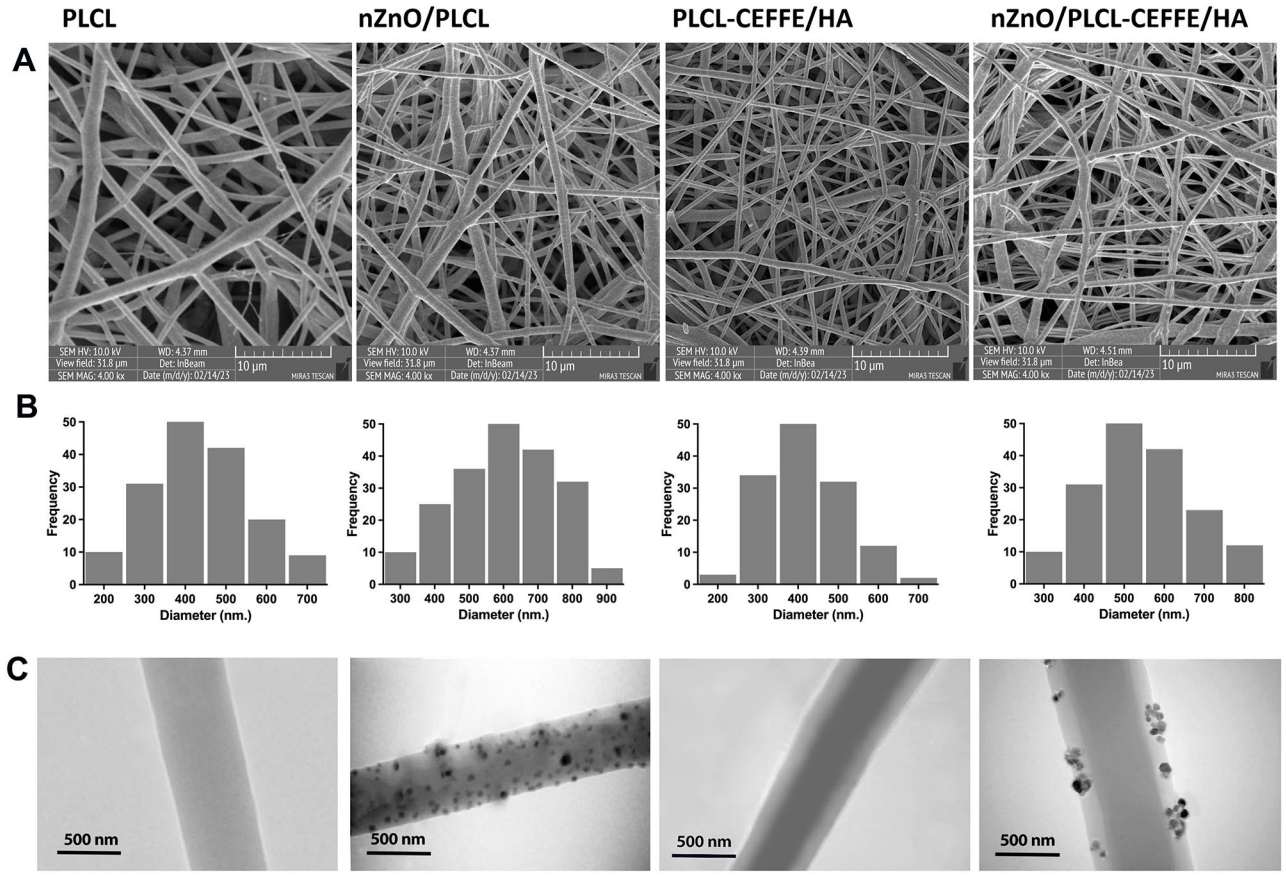

Fig. 4 Morphology and size characterization of nanofibers. (**A**) FE-SEM images with (**B**) diameter distribution of PLCL, nZnO/PLCL, PLCL-CEFFE/HA, and nZnO/PLCL-CEFFE/HA. (**C**) TEM images of the fabricated fibers

individual particles and clusters. The core-shell structure in PLCL-CEFFE/HA and nZnO/PLCL-CEFFE/HA is clearly visible, indicating effective co-axial electrospinning and successful loading of CEFFE within the core, consistent with similar coaxial electrospinning studies [32, 34].

XRD

The XRD patterns of HA, nZnO, and electrospun fiber membranes composed of PLCL, nZnO, HA, and CEFFE are depicted in the Fig. 5A. A detailed analysis of the XRD patterns provides valuable insights into the structural properties and interactions of these materials within the composite membranes. The XRD pattern of pure HA shows a broad peak around 28° indicating its semi-crystalline nature. This broad peak is characteristic of the amorphous regions within the polymer matrix, suggesting a lower degree of crystallinity typical for biopolymers like HA. nZnO exhibit a highly crystalline structure as evidenced by the presence of multiple sharp peaks in the XRD pattern. The prominent peaks at 3°, 34°, and 36° correspond to the (100), (002), and (101) planes, respectively, of the hexagonal wurtzite structure of ZnO. These peaks confirm the high crystallinity and purity of the nZnO used in this study. The XRD pattern of PLCL shows characteristic peaks at 16° and 22°, indicative of its semi-crystalline nature. These peaks correspond to the (110) and (200) planes of PLCL, respectively. The relatively broad peaks suggest a lower degree of crystallinity, which is typical for this type of polymer. The XRD pattern of the nZnO/PLCL composite shows characteristic peaks of both PLCL and nZnO. The peaks of nZnO are visible at 31°, 34°, and 36°, indicating successful loading of nZnO into the PLCL matrix. The absence of new peaks suggests that the interaction between nZnO and PLCL is primarily physical, likely through hydrogen bonding, rather than chemical interaction. In the PLCL-HA composite, the XRD pattern displays the characteristic peaks of PLCL and a broad peak of HA around 28°. This indicates the presence of HA in the composite without forming new crystalline phases, suggesting a physical mixture of HA and PLCL. Finally, he XRD pattern of the nZnO/PLCL-CEFFE/HA composite shows peaks corresponding to PLCL, nZnO, and the broad peak of HA. Notably,

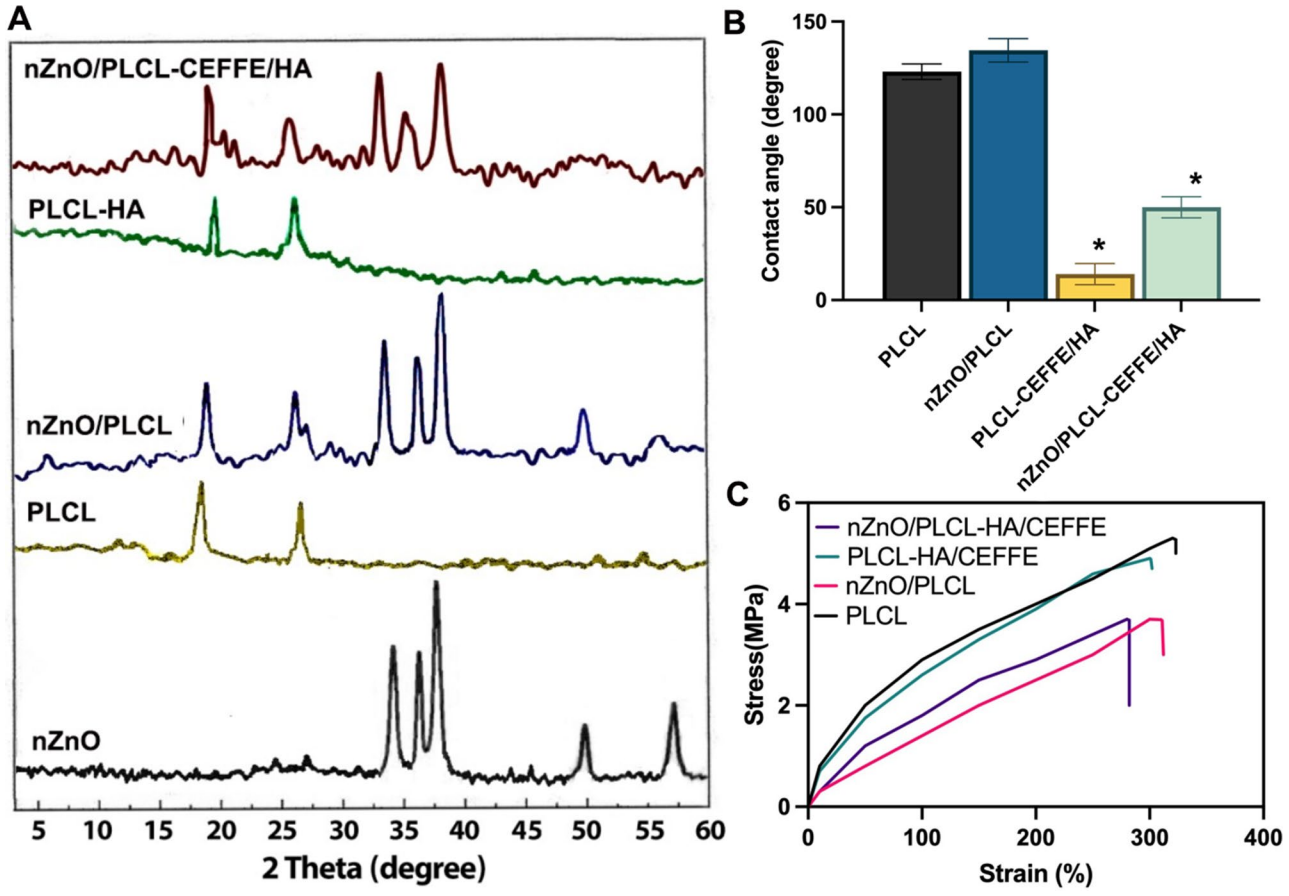

Fig. 5 Physicochemical characterization of electrospun nanofibers. (**A**) the XRD patterns of HA, nZnO, and electrospun fiber membranes composed of PLCL, nZnO, HA, and CEFFE, (**B**) Water contact angle of the various electrospun fibers, and (**C**) typical stress-strain curve of various electrospun nanofibers. $n = 3$, $^{*}p < 0.05$ vs. Control

the representative peak of PLCL at 22° is more intensified, which can be attributed to the presence of CEFFE. This intensified peak suggests that CEFFE is effectively incorporated into the composite, enhancing the crystallinity of PLCL. The absence of new peaks indicates that there is no chemical interaction among PLCL, nZnO, and CEFFE, further supporting the hypothesis of physical interaction.

Water contact angle

The hydrophilicity of the fabricated membranes was evaluated by measuring the water contact angle (Fig. 5B). The PLCL membrane exhibited a hydrophobic nature with a contact angle of approximately 121.73°. The incorporation of nZnO into the PLCL membrane (nZnO/PLCL) resulted in a further increase in the contact angle to 132.06°, indicating enhanced hydrophobicity, although this increase was not statistically significant ($p > 0.05$). In contrast, the core-shell membrane containing CEFFE and HA (PLCL-CEFFE/HA) demonstrated a drastic reduction in the contact angle to 21.85°, reflecting a highly hydrophilic surface. This significant decrease can be attributed to the presence of HA in the core, which is known for its hydrophilic properties. The addition of nZnO to the shell of the core-shell membrane (nZnO/PLCL-CEFFE/HA) resulted in a slight increase in the contact angle to 59.92°. Despite this increase, the membrane remained within the hydrophilic range, indicating that the presence of nZnO does not significantly hinder the hydrophilicity imparted by HA and CEFFE in the core.

The evaluation of hydrophilicity through contact angle measurements provides critical insights into the surface properties of the fabricated membranes. The contact angle data indicates that the incorporation of nZnO into PLCL membranes increases their hydrophobicity, while the inclusion of hydrophilic components such as HA and CEFFE significantly enhances hydrophilicity. Comparing these findings with existing literature, it is evident that the integration of hydrophilic substances like HA can effectively reduce the water contact angle and improve surface wettability. For instance, Liu et al. demonstrated that HA-modified membranes exhibited superior hydrophilicity with contact angles below 30°, consistent with our observations for the PLCL-CEFFE/HA membrane [35]. Additionally, the role of nZnO in modulating surface properties has been well-documented. Studies by Li et al. reported that nZnO enhance hydrophobicity due to their inherent surface characteristics [36], aligning with the increased contact angle observed in our nZnO/PLCL membranes. The slight increase in contact angle upon incorporating nZnO into the core-shell membrane (nZnO/PLCL-CEFFE/HA) suggests a balancing effect between the hydrophilic core and the hydrophobic nature of nZnO, which is crucial for optimizing membrane performance in biomedical applications [37]. These findings have significant implications for the design of innovative core-shell nanofiber wound dressings. The hydrophilic nature of PLCL-CEFFE/HA membranes ensures better wound exudate management, while the inclusion of nZnO provides the necessary antibacterial properties without significantly compromising hydrophilicity.

Table 1 The mechanical properties of various nanofibrous scaffolds

Sample	Tensile strength (MPa)	Elongation at bread (%)	Young's modulus (MPa)
PLCL	5.30 ± 0.42	320 ± 10	2.05 ± 0.14
nZnO/PLCL	3.75 ± 1.12	300 ± 21	1.50 ± 0.18
PLCL-CEFFE/HA	5.1 ± 0.40	293 ± 25	2.73 ± 0.21
nZnO/PLCL-CEFFE/HA	3.70 ± 1.20	280 ± 14	2.21 ± 0.11

Mchanical properties

The mechanical properties of the fabricated nanofibrous scaffolds, including PLCL, nZnO/PLCL, PLCL-CEFFE/HA, and nZnO/PLCL-CEFFE/HA, were evaluated through tensile strength tests, elongation at break measurements, and Young's modulus calculations (Fig. 5C) (Table 1). The pure PLCL scaffold exhibited the highest tensile strength of 5.30 MPa, showcasing its inherent mechanical robustness. In contrast, the addition of nZnO in the nZnO/PLCL scaffold reduced the tensile strength to 4.50 MPa, likely due to the brittle nature of nZnO, which introduces stress concentration points leading to early failure. The PLCL-CEFFE/HA scaffold displayed a tensile strength of 5.10 MPa, slightly lower than pure PLCL, indicating that CEFFE/HA did not significantly compromise the mechanical integrity of PLCL. However, the combination of nZnO and CEFFE/HA in the nZnO/PLCL-CEFFE/HA scaffold resulted in the lowest tensile strength of 3.90 MPa, suggesting a compounded effect of both modifications on the mechanical properties.

The elongation at break data followed a trend consistent with the tensile strength results. Pure PLCL demonstrated the highest elongation at break of 320%, indicative of its excellent ductility. The incorporation of nZnO resulted in a notable decrease in elongation to 250%, which can be attributed to the rigid nature of nZnO. The PLCL-CEFFE/HA scaffold showed an elongation at break of 290%, suggesting that while CEFFE/HA impacts flexibility, it does so less drastically than nZnO. The nZnO/PLCL-CEFFE/HA scaffold exhibited the lowest elongation at break of 240%, reinforcing the observation that the combination of nZnO and CEFFE/HA impairs mechanical flexibility.

Young's modulus results indicated that the addition of CEFFE/HA to PLCL increased the stiffness of the scaffold to 2.60 MPa, likely due to the reinforcing effect of

CEFFE/HA. In contrast, the addition of nZnO decreased the Young's modulus to 1.80 MPa, indicating reduced stiffness, possibly due to the introduction of stress concentrators within the polymer matrix. The nZnO/PLCL-CEFFE/HA scaffold demonstrated a moderate Young's modulus of 2.00 MPa, reflecting a balance between the stiffening effect of CEFFE/HA and the softening effect of nZnO.

In conclusion, the mechanical properties of the nZnO/PLCL-CEFFE/HA core-shell nanofibers suggest that these modifications can tailor the mechanical behavior to meet specific needs in wound healing and dressing applications. While pure PLCL and PLCL-CEFFE/HA scaffolds are suitable for applications requiring high mechanical strength and flexibility, nZnO/PLCL-CEFFE/HA scaffolds offer a balance of mechanical properties that may be beneficial for applications where moderate stiffness and additional functionalities provided by nZnO are desired.

In vitro release of nZnO and CEFFE

The release of Zn^{2+} ions from the nZnO/PLCL-CEFFE/HA core-shell electrospun nanofibers was studied using inductively coupled plasma atomic emission spectrometry (ICP-AES) (Fig. 6A). The release profile demonstrated a biphasic pattern, consisting of an initial burst release followed by a sustained release phase.

For nZnO/PLCL-CEFFE/HA core-shell nanofibers, in the first 8 h, a burst release of Zn^{2+} ions up to 630 µg was observed. This rapid release can be attributed to the presence of nZnO on the surface of the PLCL shell, which readily dissolve into the release medium. Following the initial burst, a sustained release of Zn^{2+} ions amounting to 853 µg occurred over the next 72 h. This phase likely results from the gradual degradation of the PLCL polymer matrix and the controlled diffusion of Zn^{2+} ions from the nZnO/PLCL-CEFFE/HA core-shell nanofibers. The total cumulative release of Zn^{2+} ions over a period of 96 h reached approximately 930 µg.

For the nZnO/PLCL nanofibers, a burst release of Zn^{2+} ions amounting to 330 µg/mL was noted within the initial 8 h. This is indicative of the rapid dissolution of nZnO directly exposed to the release medium. The subsequent cumulative release over the next 24 h reached 490 µg. The shorter duration of sustained release in nZnO/PLCL, compared to nZnO/PLCL-CEFFE/HA, can be attributed to the absence of the CEFFE/HA core, which provides an additional barrier and modulation effect on the Zn^{2+} release.

The biphasic release pattern observed in the nZnO/PLCL-CEFFE/HA nanofibers is advantageous for biomedical applications requiring an initial burst of antimicrobial activity followed by a prolonged release for sustained therapeutic effects. The initial burst ensures rapid disinfection, while the sustained release phase maintains a therapeutic level of Zn^{2+} ions over an extended period, which is beneficial for wound healing and tissue regeneration.

The enhanced release profile in nZnO/PLCL-CEFFE/HA compared to nZnO/PLCL highlights the significance of the core-shell structure. The CEFFE/HA core not only provides a secondary phase of Zn^{2+} release but also introduces bioactive molecules from the CEFFE, potentially offering synergistic effects in promoting tissue repair and regeneration.

The cumulative release of three key growth factors, namely bFGF, TGF-β1, and VEGF, from nZnO/PLCL-CEFFE/HA core-shell nanofibers was monitored over a period of 96 h (Fig. 6B). The release of bFGF exhibited a rapid increase during the initial 24 h, reaching approximately 150 pg/mL. This was followed by a more gradual release, achieving a maximum cumulative release of approximately 500 pg/mL by the end of the 96-hour period. The release of TGF-β1 followed a similar trend to that of bFGF but at a lower rate. Within the first 24 h,

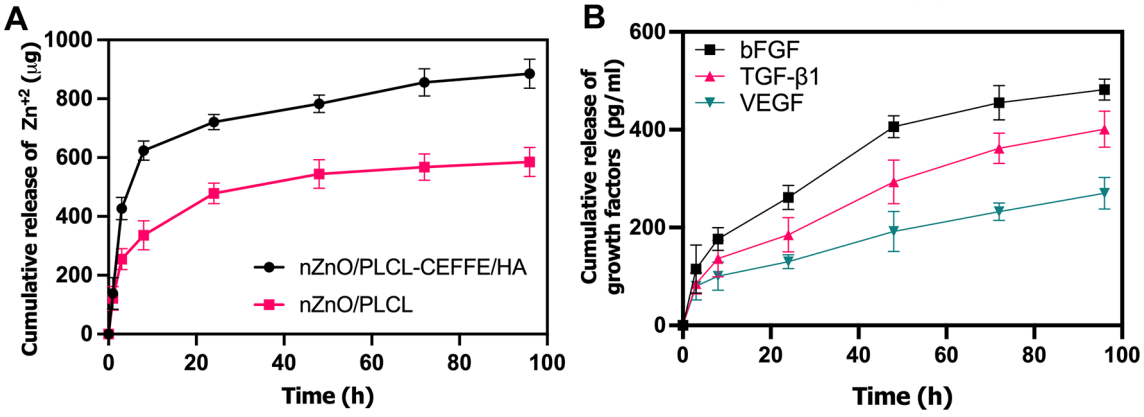

Fig. 6 Cumulative release of (A) Zn ion from nZnO/PLCL and nZnO/PLCL-CEFFE/HA, and (B) release of bFGF, TGF-β1, and VEGF from nZnO/PLCL-CEFFE/HA core-shell nanofibers. The data are presented as mean ± SD ($n = 3$)

the release reached around 100 pg/mL, with a continued steady increase over time, peaking at approximately 400 pg/mL by 96 h. Besides, the release of VEGF was slower compared to bFGF and TGF-β1. By 24 h, the release was around 75 pg/mL. The cumulative release then increased gradually, reaching a maximum of approximately 300 pg/mL by the end of the study period.

The observed release pattern of growth factors from the nZnO/PLCL-CEFFE/HA core-shell nanofibers is consistent with the expected release behavior from core-shell nanofiber systems. The slight initial burst release followed by a sustained release phase aligns well with typical core-shell nanofiber release mechanisms, confirming the effectiveness of the core-shell design in achieving controlled and prolonged delivery of growth factors.

On the other hands, the differential release rates of the growth factors are significant for tissue engineering applications. bFGF is known for its role in cell proliferation and differentiation, making its higher release rate beneficial for the initial stages of tissue regeneration. TGF-β1, with its role in matrix production and remodeling, showed a moderate release, which aligns with its function in later stages of tissue repair. VEGF, crucial for angiogenesis, exhibited the slowest release, ensuring a sustained supply for vascularization over the extended period [38].

Antibacterial activity

The antibacterial efficacy of the fabricated electrospun nanofibers was assessed against two bacterial strains: *E. coli* and *S. aureus*. The OD measurements at 600 nm after 24 h of incubation provide insight into the antibacterial properties of various nanofiber compositions.

As shown in the Fig. 7, the nZnO/PLCL and nZnO/PLCL-CEFFE/HA nanofibers demonstrated significantly lower OD values compared to the control, indicating substantial antibacterial activity. The antibacterial efficacy calculated using equation (i) shows that these nanofibers reduced bacterial growth by approximately 40% compared to the control. The presence of nZnO in these fibers likely contributed to the observed antibacterial effect, as nZnO are known for their antibacterial properties. In the case of *S. aureus*, similar to *E. coli*, the nZnO/PLCL and nZnO/PLCL-CEFFE/HA nanofibers showed a significant reduction in OD values, indicating a strong antibacterial effect. The reduction in bacterial growth was approximately 60% and 50% for nZnO/PLCL and nZnO/PLCL-CEFFE/HA, respectively. This further

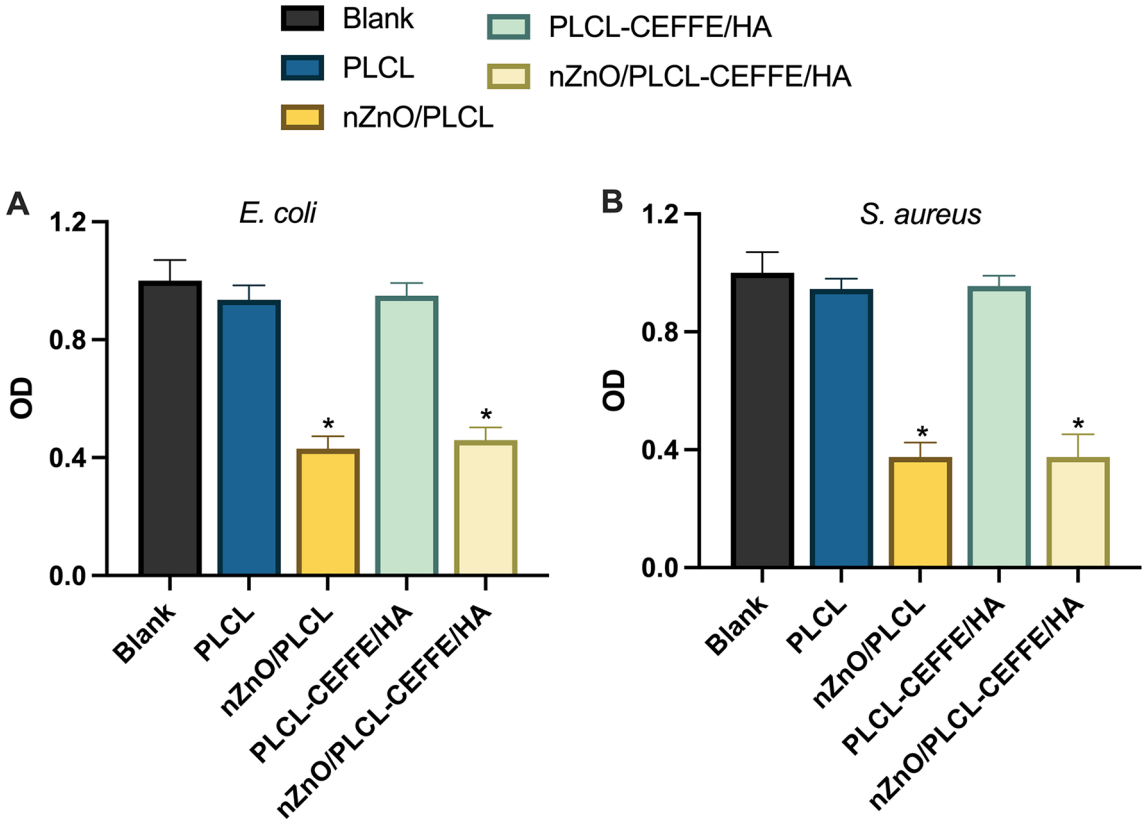

Fig. 7 Antibacterial activity against (**A**) *E.coli* and (**B**) *S. aureus* measured through turbidity method. The data are presented as mean ± SD ($n = 3$), *$p < 0.05$ vs. control was considered significant

confirms the enhanced antibacterial activity imparted by the incorporation of nZnO.

The results demonstrate that the incorporation of nZnO into PLCL nanofibers significantly enhances their antibacterial properties against both gram-negative (*E. coli*) and gram-positive (*S. aureus*) bacteria. In the case of nZnO/PLCL-CEFFE/HA nanofibers, the presence of nZnO in the shell layer is particularly effective in reducing bacterial growth. nZnO are known to induce oxidative stress and disrupt bacterial cell membranes, leading to bacterial cell death. Additionally, the use of CEFFE/HA in the core may provide further benefits for wound healing applications, potentially promoting tissue regeneration while simultaneously providing antibacterial protection.

The turbidity method is a widely recognized and reliable quantitative assay for measuring bacterial growth and inhibition, particularly in liquid cultures where planktonic bacteria are the primary focus. This method directly quantifies bacterial cell density by measuring OD at 600 nm, which is proportional to bacterial concentration. In the context of our study, where we aimed to evaluate the overall antibacterial efficacy of the nanofiber dressings against planktonic bacteria in a liquid environment, the turbidity assay provided a straightforward and accurate measure of bacterial growth inhibition. Studies have shown that turbidity assays are particularly suitable for evaluating nanoparticle-containing materials, as they allow continuous monitoring of bacterial growth in the presence of test materials, thus offering dynamic insight into the antibacterial properties over time [39].

The spread plate technique, while highly effective for assessing zone of inhibition formation on solid media, is often more suitable for materials that release antibacterial agents into the surrounding medium. In our study, the core-shell nanofiber dressings with nZnO and CEFFE were designed to maintain controlled release and localized activity. Since the antibacterial mechanism of these materials relies on the sustained release of nZnO and the activity of the CEFFE in a wound-like environment, the liquid-based turbidity assay was chosen to simulate conditions closer to in vivo situations where bacteria exist in a planktonic state rather than as colonies on solid surfaces. Furthermore, some studies suggest that the spread plate method may not fully capture the bactericidal activity of certain nanomaterials due to the limited diffusion of nanoparticles across the agar surface [40].

In addition, our materials include PLCL loaded with nZnO and HA loaded with CEFFE, which are designed for prolonged activity and biocompatibility in moist environments, such as wound dressings. The turbidity assay allows us to evaluate their antimicrobial efficacy over an extended period under conditions that mimic wound exudates, where bacteria are likely to remain in suspension rather than form solid colonies.

By focusing on turbidity measurements, we ensured a quantitative and reproducible assessment of the antibacterial activity across all test samples. However, future studies may explore the inclusion of additional assays, such as the spread plate technique for a comprehensive evaluation of both planktonic and biofilm-forming bacteria on solid surfaces, as seen in other comparative studies [41].

MTT

The MTT assay results depicted in the graph demonstrate the proliferation of NIH-3T3 cells on different fabricated fiber membranes over a period of 7 days (Fig. 8A). The experimental groups included control, PLCL, nZnO/PLCL, PLCL-CEFFE/HA, and nZnO/PLCL-CEFFE/HA. The data indicate a notable variation in cell growth among the different groups.

On Day 1, the OD values for all groups were relatively low, indicating minimal cell proliferation at the initial stage. By day 3, there was a significant increase in cell proliferation across all groups, with the control and PLCL groups showing higher OD values compared to the nZnO/PLCL group, suggesting that the presence of nZnO initially inhibited cell growth.

By day 7, a substantial increase in cell proliferation was observed in all groups, with the PLCL-CEFFE/HA group exhibiting the highest OD value, significantly surpassing the control, PLCL, and nZnO/PLCL groups. This indicates that the controlled release of CEFFE from the core-shell structure of PLCL-CEFFE/HA nanofibers significantly enhanced cell proliferation.

The release of growth factors from CEFFE is a key factor contributing to the increased cell proliferation observed in the PLCL-CEFFE/HA and nZnO/PLCL-CEFFE/HA groups. Growth factors such as VEGF, PDGF, and FGF present in CEFFE promote cell growth, differentiation, and migration, essential for wound healing and tissue regeneration. The controlled release of these growth factors from the core of the nanofibers provides a sustained supply, creating an optimal environment for cell proliferation over the 7-day period.

The nZnO/PLCL group consistently showed the lowest cell proliferation among the fabricated fiber membranes across all time points, suggesting that the incorporation of nZnO reduced the proliferation of NIH-3T3 cells. However, the continuous growth of cells over the 7-day period indicates that the membranes were only slightly cytotoxic, and the used concentration of nZnO did not inhibit cell proliferation entirely. In the nZnO/PLCL-CEFFE/HA group, while ZnO might initially reduce cell proliferation, the presence of growth factors from CEFFE

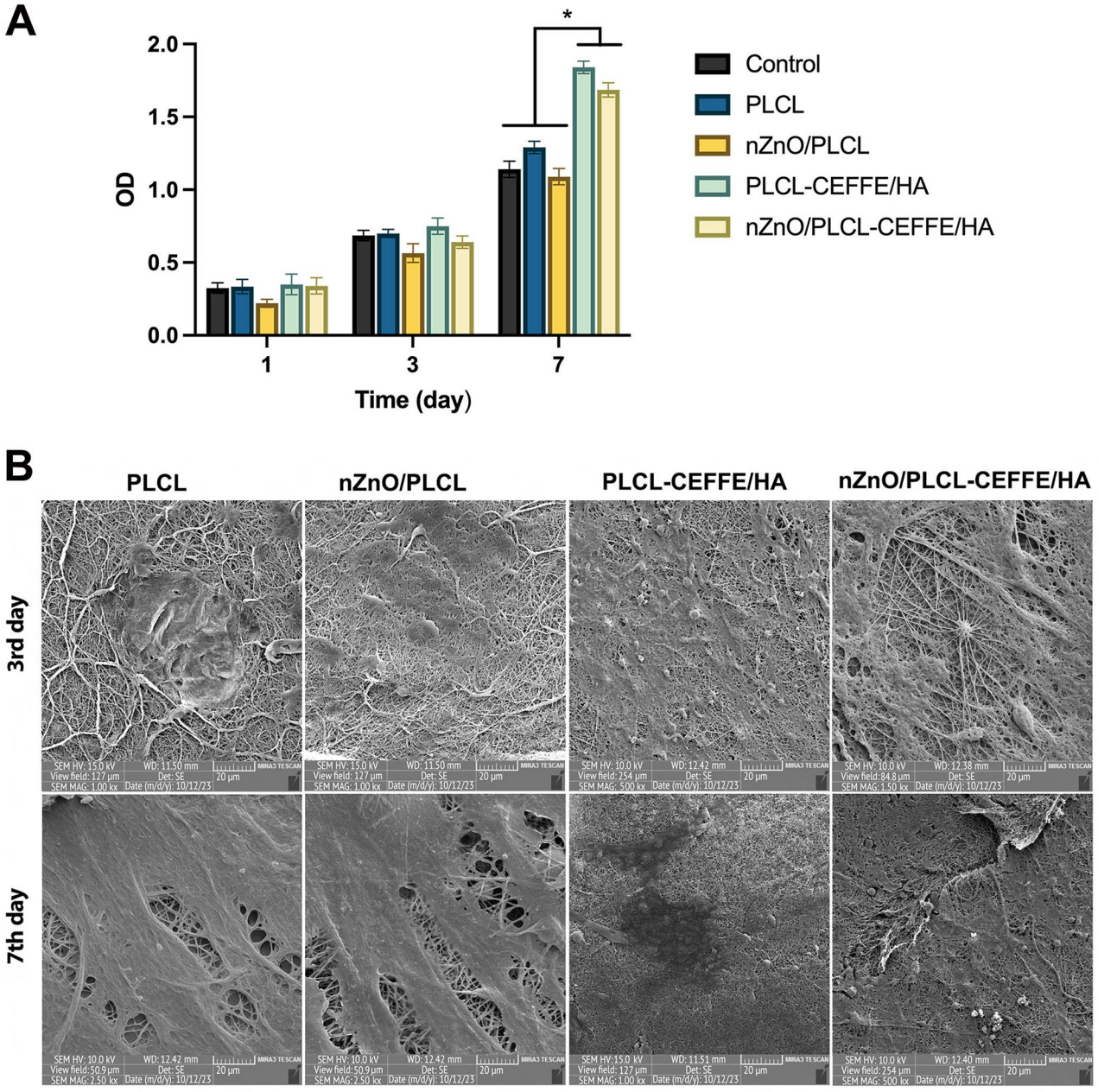

Fig. 8 Cell viability and adhesion on the various electrospun nanofibers. (**A**) graph of MTT results showing the absorbance proportional to the viability of NIH-3T3 cells, and (**B**) FE-SEM images, showing the growth of NIH-3T3 cells on fiber membrane, taken at day 4 and 7 (scale bar = 30 µm)., The data are presented as mean ± SD ($n = 3$), *$p < 0.05$

likely mitigates this effect, resulting in a net increase in cell proliferation over time.

The observed trend in cell growth can be correlated to the hydrophilicity of the membrane and the presence of nZnO. The PLCL-CEFFE/HA group's superior performance is likely due to the hydrophilic nature of CEFFE and its controlled release from the core of the nanofibers, promoting better cell adhesion and growth. Conversely, the hydrophobic nature of nZnO/PLCL may have contributed to the reduced cell proliferation observed in the nZnO/PLCL group.

FE-SEM analysis

The morphology and adhesion of NIH-3T3 cells seeded on the scaffolds were visualized using FE-SEM. The FE-SEM images captured after 4 and 7 days of culture provided insights into the cell-surface interactions (Fig. 8B). The NIH-3T3 cells showed initial adhesion and spreading on the scaffolds. The PLCL-CEFFE/HA group displayed a

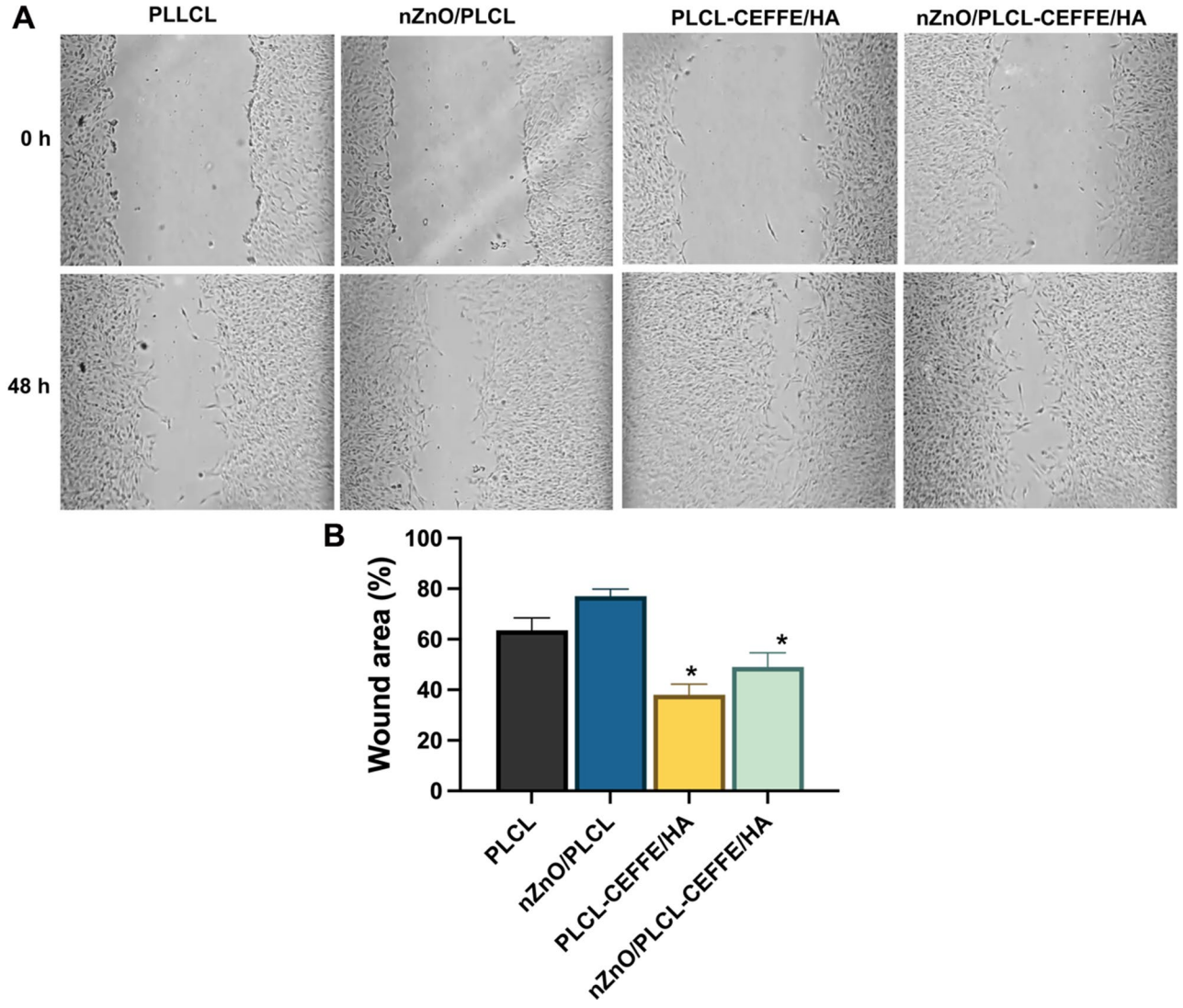

Fig. 9 Representation of cell migration performed by the scratch assay. (**A**) Scratch results showing the migration of cells co-cultured with the various electrospun nanofibers as analyzed by taken images at 0 h and 48 h. (**B**) The quantification results of the cell migration images by using the Image J software. * $p < 0.05$ vs. control was considered significant. Results are mean ± SD ($n = 3$)

more extensive cell network and better cell morphology compared to other groups, indicating that the controlled release of growth factors promoted initial cell attachment and proliferation. The nZnO/PLCL group showed less cell spreading and fewer cell extensions, supporting the MTT assay results that nZnO initially inhibited cell growth. Besides, there was a noticeable increase in cell density and spreading across all groups. The PLCL-CEFFE/HA group exhibited the most significant cell proliferation, with cells forming a dense and interconnected network. This suggests that the sustained release of growth factors from the CEFFE/HA nanofibers continued to support cell growth and proliferation. The nZnO/PLCL group, while showing improved cell adhesion compared to day 4, still had the lowest cell density among the groups, aligning with the MTT results indicating lower proliferation rates. The FE-SEM images corroborate the MTT assay results, showing that the PLCL-CEFFE/HA nanofibers provide an optimal environment for cell proliferation through the sustained release of growth factors, while the nZnO/PLCL nanofibers, despite being slightly cytotoxic, do not entirely inhibit cell growth.

In vitro scratch assay

The *in vitro* scratch assay was employed to evaluate the impact of various nanofiber formulations on the migration of NIH-3T3 cells. The wound area percentages were calculated after 48 h of incubation for each treatment group. The results are presented in the Fig. 9. The PLCL group exhibited a wound area percentage of approximately 60%, indicating moderate cell migration. The nZnO/PLCL group showed a higher wound

area percentage of around 80%, suggesting a lower efficacy in promoting cell migration compared to PLCL alone. The PLCL-CEFFE/HA group demonstrated a significantly reduced wound area percentage of about 40%, highlighting its superior performance in facilitating cell migration and wound healing. Finally, the nZnO/PLCL-CEFFE/HA group displayed a wound area percentage of approximately 50%, which, while better than nZnO/PLCL, did not outperform the PLCL-CEFFE/HA formulation. The in vitro scratch assay results provide insightful data regarding the wound healing efficacy of different nanofiber formulations. The PLCL-CEFFE/HA nanofiber showed the most promising results, with the lowest wound area percentage, indicating the highest level of cell migration and potential wound healing efficacy. The combination of CEFFE loaded in HA within the core appears to significantly enhance cell migration compared to the other formulations.

The released CEFFE with a variety of growth factors, which are crucial for cell proliferation and migration, likely contribute to the observed superior performance of the PLCL-CEFFE/HA formulation in promoting cell migration and wound healing. Conversely, the nZnO/PLCL formulation, which integrates nZnO into the PLCL polymer, exhibited the highest wound area percentage, suggesting that the presence of nZnO may inhibit cell migration to some extent. This finding aligns with previous studies indicating that while nZnO have antibacterial properties, their high concentration may be detrimental to cell viability and migration. The nZnO/PLCL-CEFFE/HA nanofibers, while demonstrating better performance than nZnO/PLCL, did not achieve the same efficacy as PLCL-CEFFE/HA. This suggests that the beneficial effects of CEFFE/HA on cell migration may be partially counteracted by the presence of nZnO.

The novel nZnO/PLCL-CEFFE/HA core-shell nanofibers offer significant advantages over traditional wound dressings like AgNPs and hydrogel-based systems. Antimicrobial efficacy is comparable between nZnO and AgNP dressings. Both exhibit strong antibacterial activity, disrupting bacterial membranes and generating ROS. However, nZnO has lower cytotoxicity and reduced risk of bacterial resistance, making it safer for long-term use in chronic wound care. AgNPs, though effective, pose concerns regarding toxicity and resistance development with extended exposure [7, 8].

Tissue regeneration is where the core-shell nanofibers truly excel compared to AgNPs and hydrogel-based systems. Hydrogels are biocompatible and provide moisture retention, but they lack bioactive components that actively promote tissue healing [4]. By incorporating CEFFE, rich in growth factors such as bFGF and TGF-β1, the core-shell nanofibers enhance fibroblast proliferation, ECM deposition, and wound healing. The study's results demonstrated superior cell migration and wound closure with CEFFE-loaded nanofibers, far exceeding hydrogel-based systems' passive role in wound care.

Mechanical properties of hydrogels can limit their application in large or irregular wounds due to poor structural integrity [42]. The PLCL matrix in the core-shell nanofibers balances mechanical strength and flexibility, making them more durable than hydrogel alternatives, even with the slight reduction in mechanical properties from nZnO incorporation.

A key advantage of the nZnO/PLCL-CEFFE/HA nanofibers is their biphasic release of zinc ions and growth factors, providing sustained antimicrobial activity and regenerative effects. This controlled release is more beneficial than AgNP dressings, which may overexpose tissues to silver, and hydrogel systems, which lack active bioactive delivery mechanisms.

Conclusion

In this study, we successfully developed and characterized innovative core-shell nanofiber wound dressings that synergize the therapeutic potential of nZnO and CEFFE. The preparation and analysis of CEFFE confirmed its richness in crucial growth factors such as bFGF and TGF-β1, which are essential for tissue regeneration. The incorporation of nZnO into PLCL nanofibers and their encapsulation within a core-shell structure containing CEFFE/HA demonstrated significant improvements in both antibacterial efficacy and fibroblast activity. Morphological analyses using FE-SEM and TEM revealed effective encapsulation and structural integrity, with nZnO imparting a rougher texture and increased fiber diameters. XRD patterns validated the successful integration of nZnO and CEFFE without new crystalline phase formation, suggesting physical rather than chemical interactions. Hydrophilicity tests indicated that CEFFE/HA enhanced the surface wettability of PLCL membranes, which is beneficial for wound healing applications. Mechanical property evaluations showed that while nZnO reduced tensile strength and elongation at break, CEFFE/HA maintained the mechanical robustness of the scaffolds. The biphasic release profile of Zn^{2+} ions and growth factors from nZnO/PLCL-CEFFE/HA nanofibers ensured prolonged antibacterial activity and sustained therapeutic effects, as evidenced by in vitro release studies. The antibacterial assays confirmed substantial efficacy against both gram-negative and gram-positive bacteria, with nZnO/PLCL-CEFFE/HA demonstrating significant reductions in bacterial growth. Cell proliferation and adhesion studies highlighted the superior performance of PLCL-CEFFE/HA nanofibers, promoting NIH-3T3 cell growth due to the sustained release of growth factors. The scratch assay further demonstrated the enhanced wound healing potential of these

nanofibers, with PLCL-CEFFE/HA showing the greatest efficacy in facilitating cell migration. Overall, our findings underscore the potential of nZnO/PLCL-CEFFE/HA core-shell nanofibers as multifunctional wound dressings. These nanofibers offer a balanced combination of antibacterial properties, enhanced hydrophilicity, and improved mechanical characteristics, alongside promoting tissue regeneration and wound healing. Future research should focus on optimizing the concentration and distribution of nZnO and CEFFE to further refine the mechanical and biological properties of these innovative wound dressings for specific biomedical applications.

Acknowledgements
The authors would like to thank the "Cellular and Molecular Research Center, Cellular and Molecular Medicine Research Institute, Urmia University of Medical Sciences" for their kindly cooperation.

Author contributions
AM and MB: Methodology, Investigation, Data curation, original draft preparation. MS: Methodology, Investigation, Software. YNE: Writing- review & editing. AE and MA: Formal analysis YP: Supervision, Conceptualization, Writing- review & editing.

Funding
No funding was received.

Data availability
No datasets were generated or analysed during the current study.

Declarations

Ethics approval and consent to participate
Not applicable.

Consent for publication
Not applicable.

Competing interests
The authors declare no competing interests.

Author details
[1]Department of Medical Microbiology, Faculty of Medicine, Ataturk University, Erzurum, Turkey
[2]Department of Biochemistry, Faculty of Medicine, Ataturk University, Erzurum, Turkey
[3]Department of Life Sciences and Health, Paris-Saclay University, Orsay, France
[4]ERNAM-Nanotechnology Research and Application Center, Erciyes University, Kayseri, Turkey
[5]Immunogenetics Research Center, Department of Tissue Engineering and Applied Cell Sciences, Faculty of Advanced Technologies in Medicine, Mazandaran University of Medical Sciences, Sari, Iran
[6]Cellular and Molecular Research Center, Cellular and Molecular Medicine Research Institute, Urmia University of Medical Sciences, Urmia, Iran

Received: 1 August 2024 / Accepted: 21 April 2025
Published online: 19 May 2025

References

1. Hamed SH, Azooz EA, Al-Mulla EAJ. Nanoparticles-assisted wound healing: a review. Nano Biomed Eng. 2023;15(4):425–35.
2. Bian D, Pilehvar Y, Kousha S, Bi J. Bioactive wound healing 3D structure based on Chitosan hydrogel loaded with Naringin/Cyclodextrin inclusion nanocomplex. ACS Omega. 2024;9(9):10566–76.
3. Pilehvar-Soltanahmadi Y, Dadashpour M, Mohajeri A, Fattahi A, Sheervalilou R, Zarghami N. An overview on application of natural substances incorporated with electrospun nanofibrous scaffolds to development of innovative wound dressings. Mini Rev Med Chem. 2018;18(5):414–27.
4. Wang X, Hu R, Han L, Lu X. Multifunctional hydrogels for chronic wounds repairing. Biosurface Biotribology. 2023;9(4):85–100.
5. Dakal TC, Kumar A, Majumdar RS, Yadav V. Mechanistic basis of antimicrobial actions of silver nanoparticles. Front Microbiol. 2016;7:1831.
6. Ahmad SA, Das SS, Khatoon A, Ansari MT, Afzal M, Hasnain MS, Nayak AK. Bactericidal activity of silver nanoparticles: A mechanistic review. Mater Sci Energy Technol. 2020;3:756–69.
7. Vivcharenko V, Trzaskowska M, Przekora A. Wound dressing modifications for accelerated healing of infected wounds. Int J Mol Sci. 2023;24(8):7193.
8. Yousefian F, Hesari R, Jensen T, Obagi S, Rgeai A, Damiani G, et al. Antimicrobial wound dressings: a concise review for clinicians. Antibiotics. 2023;12(9):1434.
9. Shahrousvand M, Mirmasoudi SS, Pourmohammadi-Bejarpasi Z, Feizkhah A, Mobayen M, Hedayati M et al. Polyacrylic acid/polyvinylpyrrolidone hydrogel wound dressing containing zinc oxide nanoparticles promote wound healing in a rat model of excision injury. Heliyon. 2023;9(8).
10. Malakar C, Kashyap B, Kalita MC, Deka S. Wound healing efficacy of rhamnolipid-coated zinc oxide nanoparticle along with its in vivo antibacterial efficacy against Staphylococcus aureus. Exp Dermatol. 2023;32(2):154–64.
11. Zamani R, Aval SF, Pilehvar-Soltanahmadi Y, Nejati-Koshki K, Zarghami N. Recent advances in cell electrospining of natural and synthetic nanofibers for regenerative medicine. Drug Res. 2018;68(08):425–35.
12. Sadeghi-Soureh S, Jafari R, Gholikhani-Darbroud R, Pilehvar-Soltanahmadi Y. Potential of Chrysin-loaded PCL/gelatin nanofibers for modulation of macrophage functional Polarity towards anti-inflammatory/pro-regenerative phenotype. J Drug Deliv Sci Technol. 2020;58:101802.
13. Zamani R, Pilehvar-Soltanahmadi Y, Alizadeh E, Zarghami N. Macrophage repolarization using Emu oil-based electrospun nanofibers: possible application in regenerative medicine. Artificial cells, nanomedicine, and biotechnology. 2018;46(6):1258–65.
14. Salih RM, Kadhim HJ. Nanofiber composite for anti-bacterial application by electrospinning technique. Kuwait J Sci. 2023;50(3):262–70.
15. Chinijani TH, Afza S, Yousefiasl S, Manoochehri H, Pourmotabed S, Arabestani M, et al. Equisetum arvense and nano zinc oxide-infused Polycaprolactone scaffolds: A multifaceted approach for antibacterial, antioxidant, and hemocompatible wound dressing. Polym Eng Sci. 2024;64(8):3455–72.
16. Güldiken ÇG, Karaosmanoğlu O, Sivas H, Gerçel HF. ZnO microparticle-loaded Chitosan/poly (vinyl alcohol)/acacia gum nanosphere-based nanocomposite thin film wound dressings for accelerated wound healing. J Appl Polym Sci. 2020;137(10):48445.
17. Rashedi SM, Rashidi A, Rahimi MK, Bahador A. Novel PLA/ZnO nanofibrous nanocomposite loaded with Tranexamic acid as an effective wound dressing: in vitro and in vivo assessment. Iran J Biotechnol. 2021;19(3):e2737.
18. Yin M, Wang X, Yu Z, Wang Y, Wang X, Deng M, et al. γ-PGA hydrogel loaded with cell-free fat extract promotes the healing of diabetic wounds. J Mater Chem B. 2020;8(36):8395–404.
19. Wang X, Deng M, Yu Z, Cai Y, Liu W, Zhou G, et al. Cell-free fat extract accelerates diabetic wound healing in Db/db mice. Am J Translational Res. 2020;12(8):4216.
20. Fang Y, Zhu X, Wang N, Zhang X, Yang D, Nie J, Ma G. Biodegradable core-shell electrospun nanofibers based on PLA and γ-PGA for wound healing. Eur Polymer J. 2019;116:30–7.
21. Singh B, Kim J, Shukla N, Lee J, Kim K, Park M-H. Smart delivery platform using Core–Shell nanofibers for sequential drug release in wound healing. ACS Appl Bio Mater. 2023;6(6):2314–24.
22. Liu M, Zhang D, Zhou X, Duan J, Hu Y, Zhang W, et al. Cell-free fat extract improves ovarian function and fertility in mice with premature ovarian insufficiency. Stem Cell Res Ther. 2022;13(1):320.
23. Huang K, Khalaji MS, Yu F, Xie X, Zhu T, Morsi Y, et al. Multifunctional bioactive core-shell electrospun membrane capable to terminate inflammatory cycle and promote angiogenesis in diabetic wound. Bioactive Mater. 2021;6(9):2783–800.
24. Shah SS, Mithoefer K. Current applications of growth factors for knee cartilage repair and osteoarthritis treatment. Curr Rev Musculoskelet Med. 2020;13:641–50.
25. Ding X, Gao J, Yu X, Shi J, Chen J, Yu L, et al. 3D-printed porous scaffolds of hydrogels modified with TGF-β1 binding peptides to promote in vivo

cartilage regeneration and animal gait restoration. ACS Appl Mater Interfaces. 2022;14(14):15982–95.
26. Vadalà G, Russo F, Musumeci M, Giacalone A, Papalia R, Denaro V. Targeting VEGF-A in cartilage repair and regeneration: state of the Art and perspectives. J Biol Regul Homeost Agents. 2018;32(6 Suppl 1):217–24.
27. Sasan S, Molavi AM, Moqadam KH, Farrokhi N, Oroojalian F. Enhanced wound healing properties of biodegradable PCL/alginate core-shell nanofibers containing Salvia abrotanoides essential oil and ZnO nanoparticles. Int J Biol Macromol. 2024;279:135152.
28. Vu TV, Nguyen TV, Tabish M, Ibrahim S, Hoang THT, Gupta RK, et al. Waterborne ZnO/acrylic nanocoating: fabrication, characterization, and properties. Polymers. 2021;13(5):717.
29. Zhang H, Yan J, Ma Q, Lin L, Pilehvar Y, Zarghami N et al. Sodium alginate hydrogels co-encapsulated with cell free fat extract-loaded core-shell nanofibers and menstrual blood stem cells derived exosomes for acceleration of articular cartilage regeneration. Int J Biol Macromol. 2024:135851.
30. Rezaei A, Katoueizadeh E, Zebarjad SM. Investigating of the influence of zinc oxide nanoparticles morphology on the properties of electrospun Polyvinyl alcohol/chitosan (PVA/CS) nanofibers. J Drug Deliv Sci Technol. 2023;86:104712.
31. Ryu YS, Kim IS, Kim SH. Effect of modified ZnO nanoparticle on the properties of polylactide ultrafine fibers. J Appl Polym Sci. 2019;136(18):47446.
32. Zhang C-L, Yu S-H. Nanoparticles Meet electrospinning: recent advances and future prospects. Chem Soc Rev. 2014;43(13):4423–48.
33. Kim JH, Joshi MK, Lee J, Park CH, Kim CS. Polydopamine-assisted immobilization of hierarchical zinc oxide nanostructures on electrospun nanofibrous membrane for photocatalysis and antimicrobial activity. J Colloid Interface Sci. 2018;513:566–74.
34. Kim G-M, Le KHT, Giannitelli SM, Lee YJ, Rainer A, Trombetta M. Electrospinning of PCL/PVP blends for tissue engineering scaffolds. J Mater Science: Mater Med. 2013;24:1425–42.
35. Liu M, Chen W, Fu J, Wang A, Ding M, Zhang L, et al. Hyaluronic acid-modified nanofiltration membrane for ultrahigh water permeance and efficient rejection of PFASs. Process Saf Environ Prot. 2022;166:214–21.
36. Li Y-J, Chen G-E, Xie H-Y, Chen Z, Xu Z-L, Mao H-F. Increasing the hydrophilicity and antifouling properties of polyvinylidene fluoride membranes by doping novel nano-hybrid ZnO@ ZIF-8 nanoparticles for 4-nitrophenol degradation. Polym Test. 2022;113:107613.
37. Pearce AK, O'Reilly RK. Polymers for biomedical applications: the importance of hydrophobicity in directing biological interactions and application efficacy. Biomacromolecules. 2021;22(11):4459–69.
38. An Y, Liu W, Xue P, Ma Y, Zhang L, Zhu B, et al. Autophagy promotes MSC-mediated vascularization in cutaneous wound healing via regulation of VEGF secretion. Cell Death Dis. 2018;9(2):58.
39. Jaberi AKH, Copaci E, Mernea M, Al-Shammari RSS, Cinteza LO. Synthesis and characterization of zein-chromium nanoparticles with antibacterial effects. Rom Biotechnol Lett. 2020;25(3):1628–34.
40. Gupta S, SK K, Kudipady ML, Puttaiahgowda YM. Antibacterial effect of copper oxide nanoparticles on Polyvinyl Chloride-Based polymer nanocomposite. Adv Polym Technol. 2024;2024(1):5527195.
41. Baruah PK, Chakrabartty I, Mahanta DS, Rangan L, Sharma AK, Khare A. Efficacy of cellulose paper treated with Cu and ag oxide nanoparticles synthesized via pulsed laser ablation in distilled water in the annihilation of bacteria from contaminated water. Rev Sci Instrum. 2020;91(3).
42. Staruch RM, Glass GE, Rickard R, Hettiaratchy SP, Butler PE. Injectable pore-forming hydrogel scaffolds for complex wound tissue engineering: designing and controlling their porosity and mechanical properties. Tissue Eng Part B: Reviews. 2017;23(2):183–98.

Publisher's note